JGR Space Physics

RESEARCH ARTICLE
10.1029/2022JA030502

Key Points:

- With time-modified indices, the effects of substorm injection and solar wind ram pressure on chorus wave generation are separately studied
- During substorm injections (large AE^*), chorus waves are primarily generated in the midnight through dawn to noon sectors near the equator
- During large P_d^*, the chorus is preferentially observed in the noon sector with a wide range of magnetic latitudes

Correspondence to:

X. Gao and H. Chen,
gaox1@mail.ustc.edu.cn;
huayue_chen@foxmail.com

Citation:

Ma, J., Gao, X., Chen, H., Tsurutani, B. T., Ke, Y., Chen, R., & Lu, Q. (2022). The effects of substorm injection of energetic electrons and enhanced solar wind ram pressure on whistler-mode chorus waves: A statistical study. *Journal of Geophysical Research: Space Physics*, *127*, e2022JA030502. https://doi.org/10.1029/2022JA030502

Received 27 MAR 2022
Accepted 16 OCT 2022

The Effects of Substorm Injection of Energetic Electrons and Enhanced Solar Wind Ram Pressure on Whistler-Mode Chorus Waves: A Statistical Study

Jiuqi Ma[1,2,3], Xinliang Gao[1,2,3], Huayue Chen[1,2,3], Bruce T. Tsurutani[4], Yangguang Ke[1,2,3], Rui Chen[1,2,3], and Quanming Lu[1,2,3]

[1]Deep Space Exploration Laboratory, School of Earth and Space Sciences, University of Science and Technology of China, Hefei, China, [2]CAS Center for Excellence in Comparative Planetology, CAS Key Laboratory of Geospace Environment, University of Science and Technology of China, Hefei, China, [3]Collaborative Innovation Center of Astronautical Science and Technology, Hefei, China, [4]Retired, Pasadena, CA, USA

Abstract Whistler-mode chorus waves in the inner magnetosphere are typically excited by an electron temperature anisotropy. The anisotropy can be driven by two sources: particle injections from the tail (such as during substorms) and the solar wind ram pressure on the dayside magnetosphere. Based on 5 years of data from Van Allen Probe A, we have separately studied the effects of substorm injection of energetic ~10–100 keV electrons and their gradient and curvature drifts (AE^*) and enhanced solar wind ram pressure (P_d^*) on the generation of whistler-mode chorus waves. We use time-modified AE^* and P_d^* indices to take into account time delays. We find that during the period of large AE^* but small P_d^*, chorus waves are mainly observed in the midnight through dawn to noon sectors ($00 \le \text{MLT} \le 13$) near the magnetic equator ($|\text{MLAT}| < 10°$) at $L = 4.5$–6.5. With an increase in AE^*, both the chorus occurrence rates and the wave amplitudes increase. While under the condition of enhanced P_d^* but small AE^*, chorus waves are preferentially detected on the dayside ($07 \le \text{MLT} \le 14$) in a wide range of latitudes ($|\text{MLAT}| < 20°$) at outer L-shells ($L = 5.5$–6.5). With the increase of P_d^*, chorus occurrence rates also increase, while the amplitude remains relatively constant. Our study supports the two mechanisms for chorus excitation in the Earth's magnetosphere and provides a better understanding of the global distribution and properties of chorus waves.

1. Introduction

Whistler-mode chorus waves are one of the most common electromagnetic emissions in the Earth's magnetosphere, typically falling in the frequency range of 0.1–0.8 f_{ce} (f_{ce} is the equatorial electron cyclotron frequency). Their frequency spectra are typically divided into two frequency bands, that is, upper band and lower band, separated by a power minimum near 0.5 f_{ce} (Burtis & Helliwell, 1976; H. Chen et al., 2021; H. Y. Chen, Gao, et al., 2022; Gao et al., 2014a, 2018, 2019; Koons & Roeder, 1990; Li et al., 2012; Thorne, 2010; Tsurutani & Smith, 1974, 1977). In the magnetosphere, chorus waves are usually composed of a series of discrete and repetitive elements (H. Y. Chen, Lu, et al., 2022; R. Chen et al., 2022; Gao et al., 2014a; Helliwell, 1965; Lu et al., 2021; Tsurutani et al., 2020). Chorus waves are well known for their importance in controlling the radiation belt dynamics. They not only are responsible for accelerating electrons with energy of ~100 keV to relativistic (>1 MeV) energies (Hajra et al., 2015; Thorne et al., 2013; Tu et al., 2014) but also can scatter ~10 keV electrons into the loss cone, causing the electron precipitation into the upper atmosphere to form microbursts, and pulsating and diffuse auroras (Nishimura et al., 2010; Thorne et al., 2010; Tsurutani et al., 2013).

It is accepted that two separate mechanisms cause the excitation of chorus waves in the Earth's magnetosphere: energetic ~10–100 keV electron injections during the substorm plus gradient and curvature drift (Li, Thorne, Angelopoulos, Bonnell, et al., 2009; Meredith et al., 2003; Miyoshi et al., 2007; Tsurutani & Smith, 1974, 1977; Tsurutani, Church, et al., 1979; Tsurutani, Smith, et al., 1979) and enhanced solar wind ram pressure (Fu et al., 2012; Gail & Inan, 1990; Gail et al., 1990; Keika et al., 2012; Salvati et al., 2000). DeForest and McIlwain (1971) have shown that ~100 eV to 1 keV plasma sheet electrons are injected into the nightside magnetosphere during substorms. These injected charged particles conserve the first two adiabatic invariants, which lead to particle energization to ~10–100 keV and a temperature anisotropy ($T_\parallel < T_\perp$, where $T_\parallel$ and $T_\perp$ are parallel and perpendicular temperatures with respect to the background magnetic field) of energetic electrons (Gao et al., 2014a; Li et al., 2010; Omura et al., 2008; Thorne & Kennel, 1967). The anisotropic electrons are unstable for the generation

of chorus waves during their eastward gradient and curvature drift from the midnight sector through dawn to local noon. Enhanced solar wind ram pressure compresses preexisting energetic electrons (∼10–100 keV), causing betatron acceleration and energizing the particles in their perpendicular temperature component. With parallel temperature remaining constant, this increases the temperature anisotropy and leads to instability (Anderson & Hamilton, 1993; Southwood & Kivelson, 1975). Several global models of chorus waves have been established by utilizing the data obtained from Ogo 5 (Tsurutani & Smith, 1977), CRRES (Meredith et al., 2003), THEMIS (Li, Thorne, Angelopoulos, Bortnik, et al., 2009), Cluster (O. V. Agapitov et al., 2015), Van Allen Probes (Wang et al., 2019), and multiple satellite observations (Meredith et al., 2012). The above observation results and models suggest that the occurrence of chorus waves strongly depends on substorm activities (i.e., AE index). Typically, chorus waves' amplitude and occurrence rate increase when substorms activities are enhanced. The amplitude of chorus waves at low magnetic latitudes has a local time dependence consistent with the eastward drift of injected electrons (Li, Thorne, Angelopoulos, Bortnik, et al., 2009; Meredith et al., 2003; Tsurutani & Smith, 1977). In this scenario, chorus waves are mainly excited near the magnetic equator, where the magnetic field reaches a minimum value (Kennel & Petschek, 1966; Tsurutani & Lakhina, 1997). Poynting flux measurements also support the equatorial source region of chorus waves (Lauben et al., 2002; LeDocq et al., 1998; Teng et al., 2018).

The dayside magnetosphere will be compressed further when the solar wind ram pressure is enhanced. This distorted configuration will cause a day–night asymmetry of the magnetosphere, which leads to energetic electron drift shell splitting (Min et al., 2010; Roederer, 1967; West et al., 1973). This effect causes further enhancement of the anisotropy of the dayside outer magnetospheric electrons, in which the ∼10–100 keV electrons are essential for the generation of the chorus waves. The dayside compression of the magnetosphere by the solar wind forms a bifurcation of the magnetic equator so that there are two "magnetic equators" that are formed at high magnetic latitudes. These have been called minimum-B pockets (Kim et al., 2008; Öztürk & Wolf, 2007; Shabansky, 1971; Tsurutani & Smith, 1977). These anisotropic electrons that drift into these "magnetic equators" can go unstable and generate the chorus if the plasma condition is suitable (Kennel & Petschek, 1966). Previous statistical results have also suggested that the chorus wave generation is relevant to the solar wind ram pressure (Aryan et al., 2014; Golden et al., 2012; Kim et al., 2013), and the amplitude of dayside chorus wave increases when solar wind ram pressure is enhanced. It is predicted that the high-latitude magnetic local minimum-B pockets should also be the source regions of chorus waves. Vaivads et al. (2007) presented a chorus event generated at the high-latitude local minimum-B pocket. Tsurutani et al. (2009) reported two high-latitude chorus events in which Poynting flux was directed toward the equator, implying that the chorus waves were generated near the minimum-B pockets at magnetic latitudes above the spacecraft.

The studies discussed above have indicated that there may be these two mechanisms for chorus generation: substorm energetic electron injection (Li, Thorne, Angelopoulos, Bortnik, et al., 2009; Meredith et al., 2003; Tsurutani & Smith, 1974, 1977) and enhanced solar wind ram pressure compressing preexisting remnant energetic electrons (Golden et al., 2012; Keika et al., 2012; Tsurutani & Smith, 1977). This study aims to analyze 5 years of Van Allen Probes' high-resolution chorus data to separate the chorus generated by the two different mechanisms. To do this, both the AE index and solar wind ram pressure P_d are modified by considering their time delays (H. Chen et al., 2020). We will determine the occurrence rates of enhanced chorus waves as a function of substorm activity and solar wind ram pressure increases. We additionally determine the local time and L-shell dependence of the chorus for two separate mechanisms.

2. Data Set and Analysis Method

The Van Allen Probes mission consists of two satellites (probe A and B) equipped with the same instruments with a perigee of ∼1.1 R_E (the Earth radius), an apogee of ∼5.8 R_E, and an inclination of 10° (Kessel et al., 2013; Mauk et al., 2013). The Electric and Magnetic Field Instrument Suite and Integrated Science (EMFISIS) suite (Kletzing et al., 2013) provided the survey-mode wave power spectrum data from 10 Hz to 12 kHz every 6 s. The low-resolution magnetic fields (64 samples/s) are measured by the fluxgate magnetometer (MAG; Kletzing et al., 2013) and here treated as the background magnetic fields, which are then used to calculate the equatorial cyclotron frequencies f_{ce}. The upper hybrid resonance frequencies measured by the high-frequency receiver (Kurth et al., 2015) can be used to estimate the plasma number densities. Moreover, the L-shell (L), magnetic latitude (MLAT), and magnetic local time (MLT) values of the satellite are estimated by the TS04 model (Tsyganenko & Sitnov, 2005). All data can be accessed from https://spdf.gsfc.nasa.gov/pub/data/rbsp.

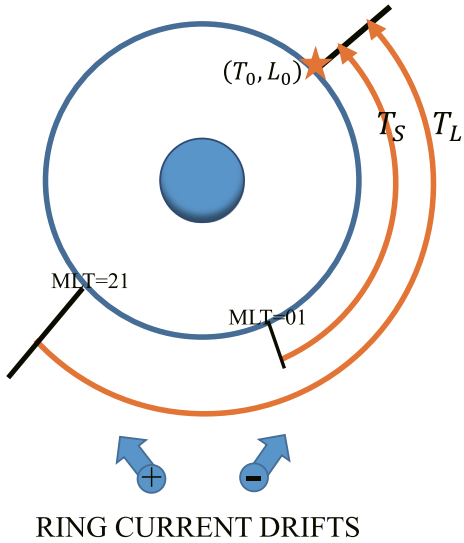

Figure 1. The diagram shows the method we used to define AE^* index.

The geomagnetic index (AE) and the solar wind ram pressure (P_d) with a resolution of 1 min have been obtained from high-resolution OMNI data set (https://omniweb.gsfc.nasa.gov). Because there is a delay from substorm onset (indicated by AE) as the energetic electron drift from midnight to the local time of chorus measurement. The AE index is modified to take the drift into account. This revised AE value is called AE^*. We follow the method in Figure 1 of H. Chen et al. (2020). The drift velocity of electrons is given as $\overrightarrow{V_{dri}} = \frac{\mu}{q\gamma}\frac{\vec{b}\times\nabla B}{B} + \frac{p_{\parallel}^2}{q\gamma m_e}\frac{\vec{b}\times(\vec{b}\cdot\nabla)\vec{b}}{B}$, where $m_e, q, \vec{b}, \mu, p_{\parallel}$, and γ indicate the mass of the electron, the charge of the electron, the unit vector of the magnetic field, the magnetic moment, the parallel momentum, and the relativistic factor, respectively. The electrons are considered to be injected from the midnight sector (MLT = 21–01; Lopez et al., 1990). Since chorus waves are commonly excited by electrons with ~10–100 keV, we set the injected electrons' kinetic energy as E_k = 25 keV, with a pitch angle of 45°. This has been used by Tsurutani and Smith (1977) and worked well. At time T_0, if a chorus event is detected at L_0 and MLT_0 (MLT_0 = 01–21), then the longest drift time T_L, meaning electrons drift from the position of MLT = 21 to satellite position, which can be given as $T_L = \frac{2\pi L_0 R_E}{V_{dri}} \times \frac{MLT_0+3}{24}$. While, the shortest drift time T_S, which means electrons drift from the position of MLT = 01 to satellite position, is estimated as $T_S = \frac{2\pi L_0 R_E}{V_{dri}} \times \frac{MLT_0-1}{24}$. The modified AE^* is then defined as the largest value in the time interval from $T_0 - T_L$ to $T_0 - T_S$. Note that if MLT_0 is in the range of 21–01, AE^* is evaluated as the largest value in the time interval of $T_0 - \frac{2\pi L_0 R_E}{V_{dri}}$ to T_0. The solar wind ram pressure data provided by the Wind and ACE satellites have been time shifted to Earth's bow shock nose. For the ram pressure, we use the largest P_d value in the previous 15 min. This is the P_d^* parameter (Liu et al., 2019).

We present a chorus wave example detected on 19 March 2015 in Figure 2, including the (c) magnetic and (d) electric spectral densities, (e) ellipticity ε, (f) wave normal angle θ, (g) the ratio Sz/S (where S is the Poynting flux and Sz is its parallel component), (h) amplitude δB, and (i) a flag "*pf*." The dashed, dotted, and solid lines in panels (c–g) represent the frequencies of f_{ce}, 0.5 f_{ce}, and 0.1 f_{ce}, respectively. The amplitude δB is the root mean square of integrated wave magnetic spectral density from 0.1 to 0.8 f_{ce}, and the *pf* is given as the power-weighted average on Sz/S. Panel (a) shows the measured and time-modified AE and P_d indices. There exist several different intervals: the interval from 7:10 to 7:30 UTC has high AE^*; the interval between 8:00 and 8:50 UTC has high P_d^*, the interval 9:10–10:00 UTC has both high AE^* and P_d^*. The solid black line in panel (b) denotes the plasma density, which is much smaller than the density threshold at the plasmapause (given by $124 \times (3/L)^4 \mathrm{cm}^{-3}$; Gao et al., 2014b; Li et al., 2016; Sheeley et al., 2001) marked by a green dashed line, suggesting this chorus wave is outside the plasmapause. The wave is propagating away from the equator (with $Sz/S \approx -1$ in the south hemisphere) and has a right-handed polarization ($\varepsilon \approx 1.0$) and a small wave normal angle ($\theta < 30°$).

3. Statistical Results

The chorus waves in the frequency range of $0.1 - 0.8 f_{ce}$ are selected from Van Allen Probe A at L = 3–7 during the period from October 2012 to December 2017, and all the waves are required to be outside the plasmapause. Since chorus waves typically have a right-hand polarization and are circularly polarized (Verkhoglyadova et al., 2010), we only record waves when ellipticity >0.7 and planarity >0.8. Additionally, only large-amplitude waves with $\delta B > 5$ pT are accepted in our study. To distinguish the effect of substorm injection and solar wind ram pressure on chorus wave excitation, we have studied how chorus wave properties depend on only one index alone by restricting the other one to quite a low value simultaneously. The chorus wave events are divided into five categories of AE^* and P_d^* indices: low AE^* and P_d^* ($AE^* < 100$ nT and $P_d^* < 1.5$ nPa), moderate AE^* but low P_d^* ($100 < AE^* < 300$ nT and $P_d^* < 1.5$ nPa), strong AE^* but low P_d^* ($AE^* > 300$ nT and $P_d^* < 1.5$ nPa), moderate P_d^* but low AE^* ($1.5 < P_d^* < 2.5$ nPa and $AE^* < 100$ nT), strong P_d^* but low AE^* ($P_d^* > 2.5$ nPa and $AE^* < 100$ nT). We define 6 s of data as a chorus event. There are 31,131, 67,855, 78,522, 52,633, and 32,350 chorus events in each category. The corresponding times are 51.88, 113.09, 130.87, 87.72, and 53.91 hr, and the dwell times of the spacecraft are 7,374.42, 3,097.31, 1,140.08, 5,444.83, and 3,142.04 hr, respectively.

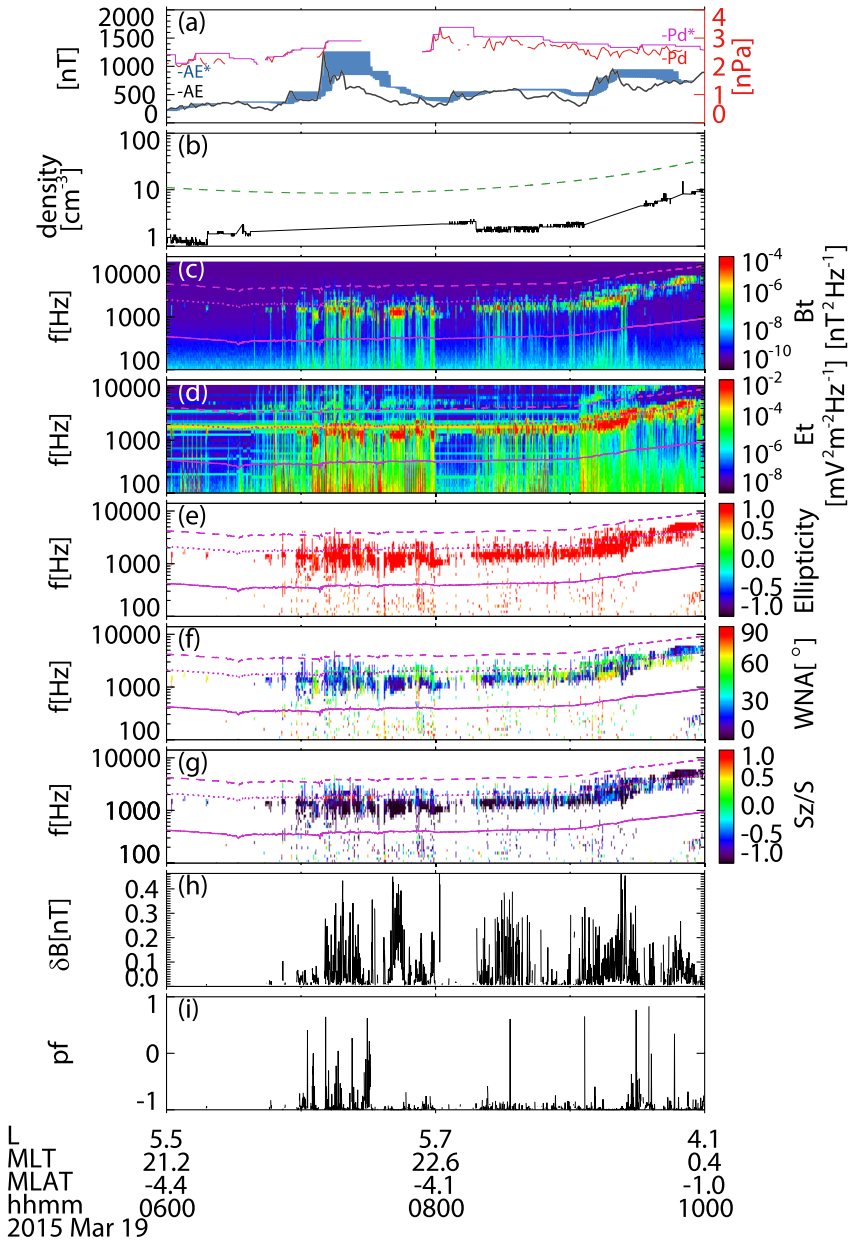

Figure 2. The overview of the chorus wave event was observed by Van Allen Probe A on 19 March 2015, including (a) the measured (black) and modified (blue) AE and measured (red) and modified (magenta) P_d indices, (b) electron density, (c) magnetic and (d) electric spectrum densities, (e) ellipticity ε, (f) wave normal angle θ, (g) the ratio Sz/S, (h) amplitude δB, and (i) "*pf*." The blue shaded area in (a) corresponds to the modified AE index, the upper edge of the shaded area is the maximum value, and the lower edge of the shaded area is the third quartile. The green dash line in (b) indicates the plasma density given by the $124 \times (3/L)^4$. In (b)–(f), the magenta lines represent $0.1 f_{ce}$ (solid), $0.5 f_{ce}$ (dotted), and f_{ce} (dashed).

Figure 3 shows the chorus wave occurrence rate distribution in the (a–c) L-MLT and (d–f) L-MLAT planes under low P_d^* ($P_d^* < 1.5$ nPa) and three different AE^* levels, with the bin size of 0.5 L × 1 MLT hr and 0.5 L × 2 MLAT deg, respectively. Here, the occurrence rate is calculated as the ratio between the wave observation time and the satellite dwell time in the same bin and category. During quiet periods when $AE^* < 100$ nT and $P_d^* < 1.5$ nPa, the wave occurrence rate is quite low and is almost uniformly distributed. As the AE^* increases (Figures 3b and 3c), the occurrence rate increases over dawn to local noon sectors ($00 \leq \text{MLT} \leq 13$) at $L = 4.5$–6.5,

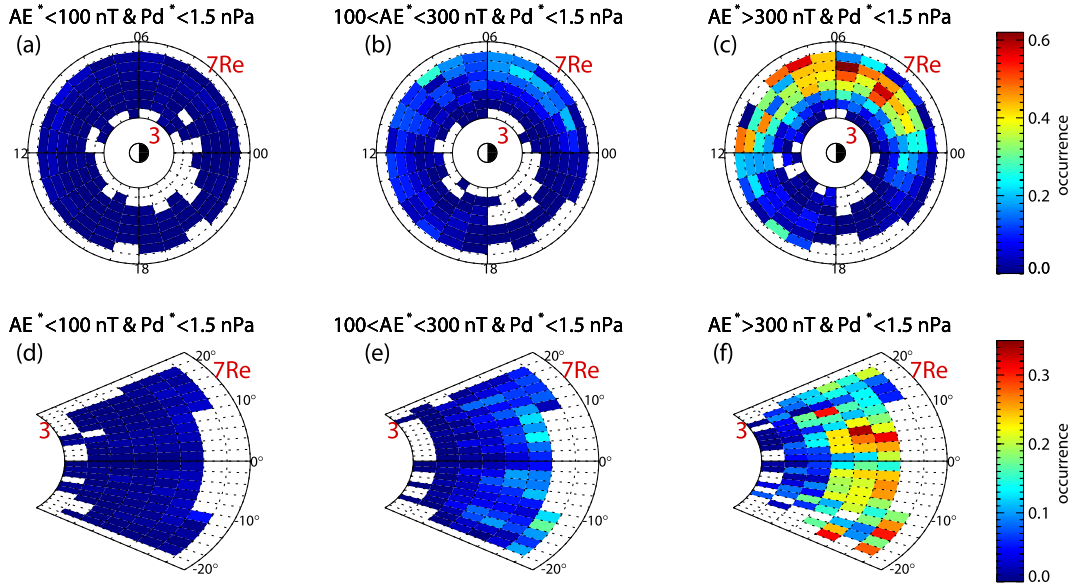

Figure 3. The chorus waves occurrence rate distribution in the (a–c) L-MLT (0.5 L × MLT) and (d–f) L-MLAT (0.5 L × 2 MLAT) planes under the low ram pressure ($P_d^* < 1.5$ nPa) and three different AE^* levels.

which is consistent with the drift path of energetic electrons. Moreover, except that several events are in the higher latitudes at large L-shell (L = 6.0–6.5), the waves are primarily observed near the equator with |MLAT| < 10° (Figures 3e and 3f).

The occurrence rates under weak injection ($AE^* < 100$ nT) and three different P_d^* levels have been shown in Figure 4. Unlike substorm injections, with the increase of solar wind ram pressure (Figures 4b, 4c and 4e and 4f), there is a clear trend that the waves are mainly detected in the noon sector (07 ≤ MLT ≤ 14) at a relatively large L-shell (L = 5.5–6.5). Moreover, the regions with relatively higher occurrence rates are away from the equator and extend to higher latitudes with |MLAT| = 10° − 20°. This suggests that the favored regions of the chorus waves generated by two potential factors are different.

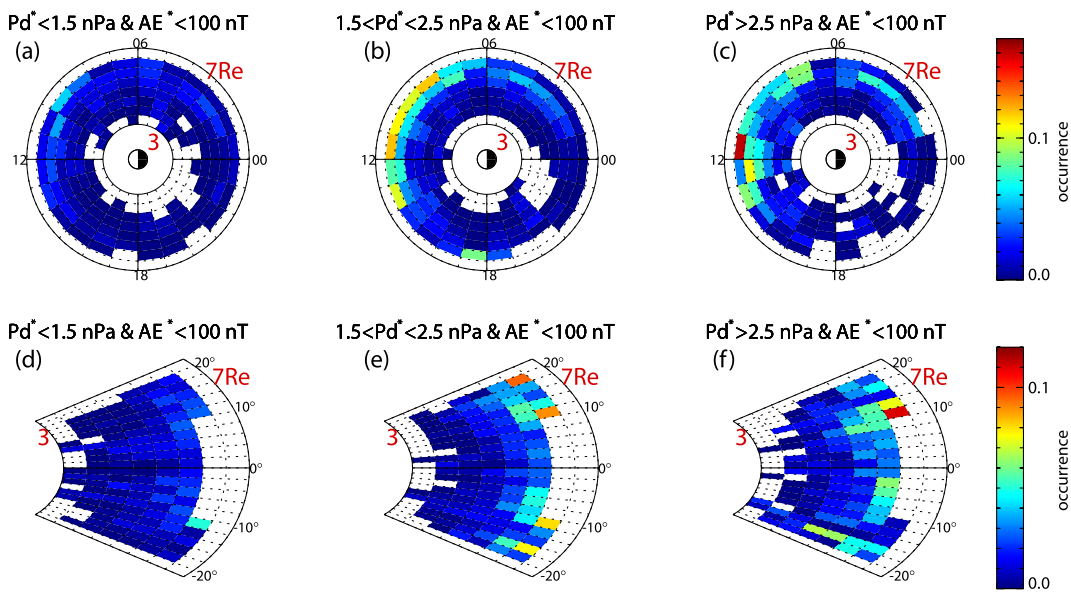

Figure 4. The distribution of the chorus waves occurrence rate in the (a–c) L-MLT and (d–f) L-MLAT planes under weak injection ($AE^* < 100$ nT) and three different P_d^* levels.

Figure 5 presents the global distribution of average normalized amplitude $(\delta B/B_0)_{avg}$ in (a, b and e, f) L-MLT and (c, d and g, h) L-MLAT planes under different conditions of AE^* and P_d^* indices. We only consider the bins containing more than 500 events to make our results statistically significant. The distribution in the quiet period has not been shown since the wave occurrence rate is quite low. During the period of high AE^* but low P_d^* (Figures 5a–5d), the intense waves are primarily detected in the midnight and dawn sectors (MLT = 00–08) at $L = 5$–6 near the equator, which is consistent with the regions with higher occurrence rates. Moreover, during the periods of strong injections (large AE^*), the waves have intense amplitudes. While under the condition of high P_d^* but low AE^* (Figures 5e–5h), the intense waves are only distributed on the dayside (MLT = 11–15) at higher latitudes ($|\text{MLAT}| > 10°$) in the outer L-shells ($L = 5.5$–6.0). However, as the solar wind ram pressure increases, the amplitudes do not increase significantly. It is possible that at larger L, beyond the limits of the VAP satellite orbits, the chorus amplitudes are much higher. However, this is beyond the efforts of the present study.

To identify the wave source region, we have further analyzed the propagating direction of the chorus waves. Figure 6 shows the average Pf_{avg} distribution in the L-MLAT planes under different conditions. Here, $Pf_{avg} = 1.0$ (-1.0) means that the Poynting flux is along (against) with the background magnetic field, and $Pf_{avg} \approx 0$ denotes the waves propagate equally in both directions. The latter can be used to identify the source region. We only show the bins with at least 500 events detected to ensure the statistics are more convincing. During the periods of strong injection (Figures 6a and 6b) and solar wind ram pressure (Figures 6c and 6d), Pf_{avg} is close to 0 near the equator, and $|Pf_{avg}| \approx 1$ as long as waves leave away the equator. This indicates that the wave source regions are near the equator under both two conditions. This is in agreement with the Kennel and Petschek (1966) theory.

4. Summary and Discussion

By using 5-year data from Van Allen Probe A, we have separately studied the effects of substorm injection (AE^*) of energetic ~10–100 keV electrons and their gradient and curvature drift to other local times and enhanced solar wind ram pressure (P_d^*) on whistler-mode chorus waves. Both AE^* and P_d^* indices have been modified to consider appropriate time delays. We find that during the period of large AE^*, chorus waves are mainly observed in the midnight through dawn to noon sectors ($00 \le \text{MLT} \le 13$) near the equator ($|\text{MLAT}| < 10°$) at $L = 4.5$–6.5. With the enhancement of AE^*, both the chorus occurrence rate and the wave amplitude increase. While under the condition of enhanced P_d^*, chorus waves are primarily observed in the noon sector ($07 \le \text{MLT} \le 14$) in a wide range of latitudes at outer L-shells ($L = 5.5$–6.5). With the enhancement of P_d^*, the occurrence rate also increases while the amplitude remains relatively constant. It is determined that the favored regions of chorus waves generated by the two drivers are quite different.

It is accepted that there may exist two potential ways to drive the excitation of whistler-mode chorus waves in the outer magnetosphere, such as substorm injection and solar wind ram pressure (Salvati et al., 2000; Spasojevic & Inan, 2010; Tsurutani & Smith, 1974, 1977). On the one hand, the energetic electrons are injected from the midnight sector during substorms, which are unstable to excite chorus waves near the equator as they drift eastward (Li et al., 2010; Omura et al., 2008; Thorne & Kennel, 1967; Tsurutani & Smith, 1977). This is consistent with the observational results in Figures 3 and 6, which show that the wave sources are basically in the midnight through dawn to noon sectors in the low latitudes. On the other hand, the enhanced solar wind ram pressure can compress the magnetic field on the dayside, making the field lines flatter, and the electrons are adiabatically heated in the perpendicular direction (Tsurutani et al., 2009). In our study, we find that under the condition of large P_d^*, the waves are preferentially observed in the noon sector in a wide range of latitudes ($|\text{MLAT}| < 20°$). But the wave source regions are still near the equator (Figure 6d) based on Van Allen Probes data. This could be an artifact due to the low L-shells accessible to the Van Allen Probes. Below 7 R_E, the minimum-B location remains at the equator, even during the high P_d^* periods. This also suggests that during large P_d^*, the waves generated near the equator can propagate to higher latitudes with relatively weaker wave damping (Lu et al., 2019; Taubenschuss et al., 2016).

As shown in Figure 5, the amplitude of chorus waves did not increase as the solar wind ram pressure increased. By using the particle data from the Helium, Oxygen, Proton, and Electron (HOPE) Mass Spectrometer (Funsten et al., 2013) onboard the Van Allen Probes, we also perform the statistical analysis on the global distribution of electron anisotropies under different conditions of AE^* and P_d^* indices (not shown). Here, the temperature anisotropy is calculated following the method of Kubota et al. (2018). However, we find the median electron anisotropy (~1) is almost independent on MLT, MLAT, AE^*, and P_d^*, which may be due to the fast relaxation of hot electrons

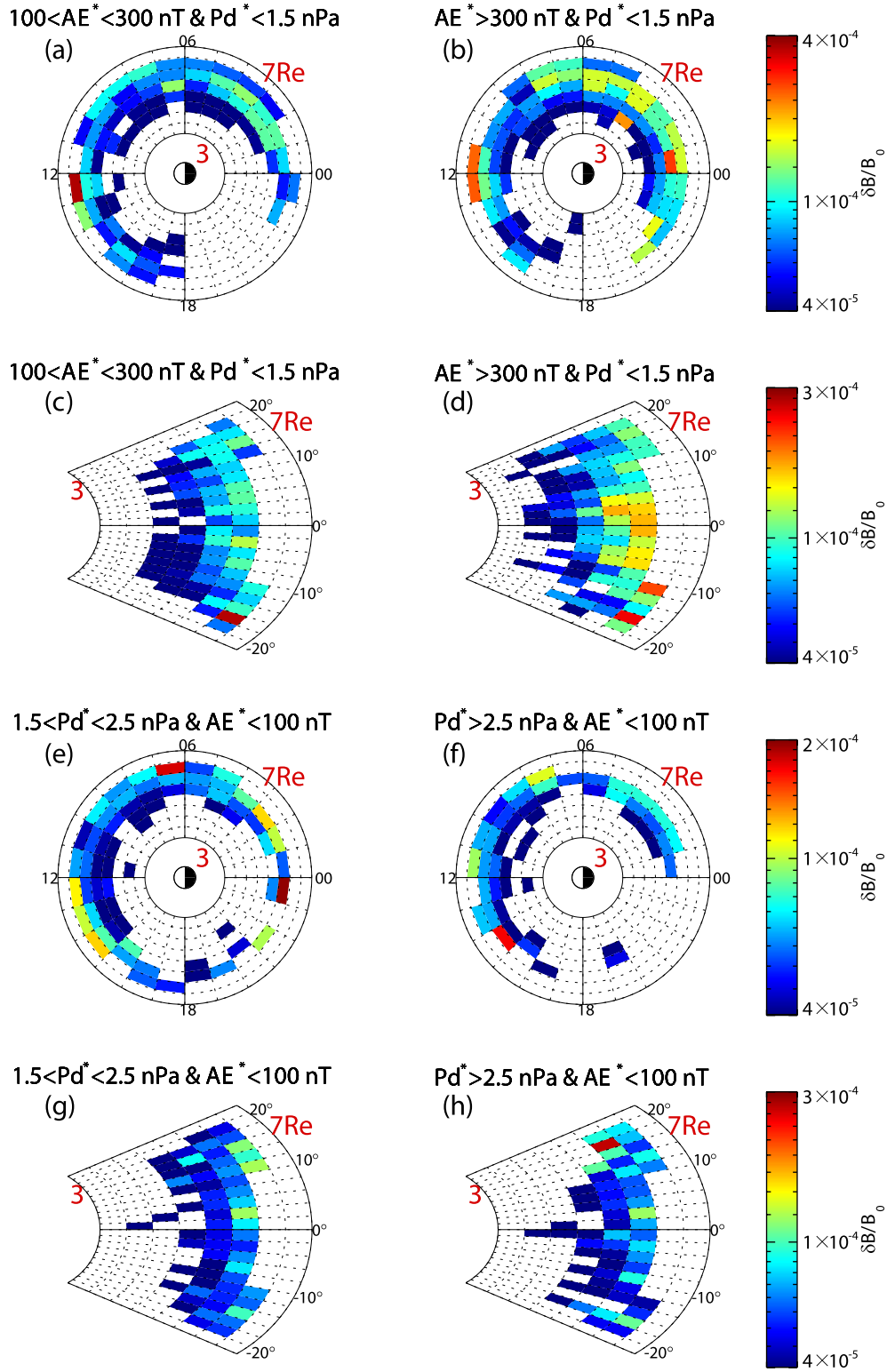

Figure 5. The distribution of average normalized amplitude $(\delta B/B_0)_{avg}$ in the (a, b and e, f) L-MLT and (c, d and g, h) L-MLAT planes under different conditions of AE^* and P_d^* indices.

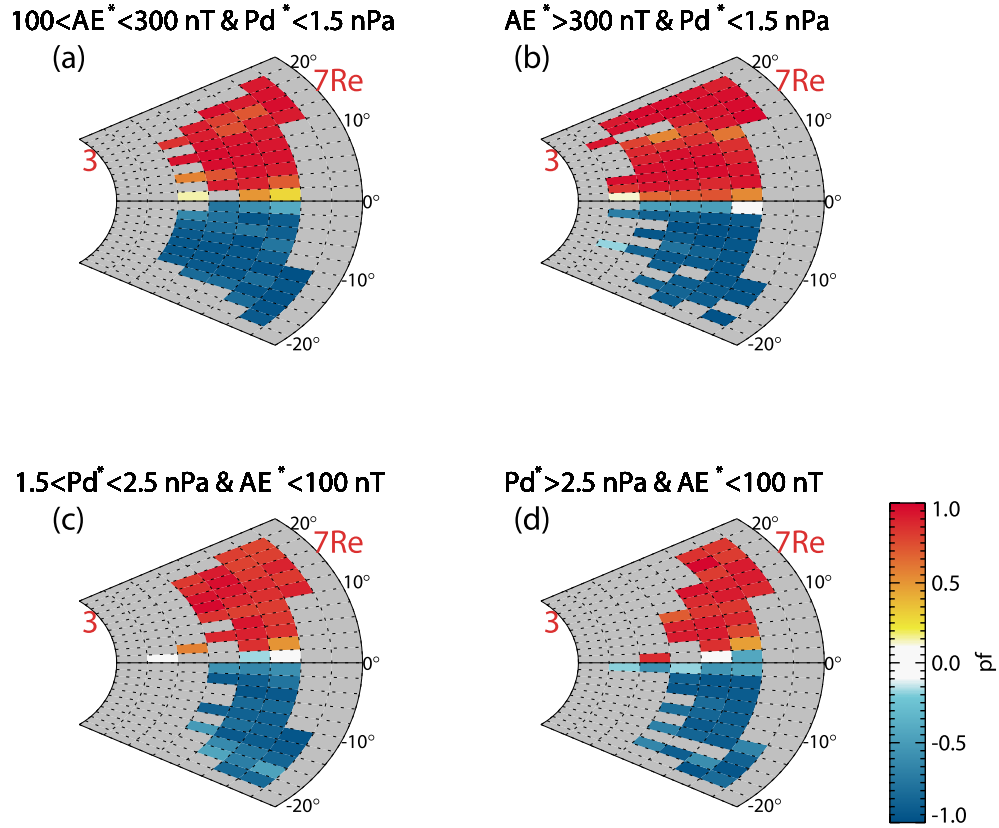

Figure 6. The distribution of average Pf_{avg} in the L-MLAT planes under different conditions.

after the wave excitation. The amplitude of chorus waves should be determined by both the linear and nonlinear processes (Gao et al., 2014a; Omura, 2021), which will depend on many plasma parameters, such as the configuration of the magnetic field, plasma density, proportion of energetic electrons, and temperature anisotropy. The other potential cause is due to the limited L range ($L < 7$) of Van Allen Probes, where the compression of solar winds may be not very strong. Nevertheless, the dependence of wave amplitude on the solar wind ram pressure remains an open question, which is left for further study.

There are some outliers in our study. For example, in Figure 3f, some events have a latitude of over 10°. In Figures 5a and 5b, some chorus events are in the noon sector. These outliers are just associated with some long-lasting chorus waves, which make the counting number of events abnormally high in such regions. In such regions, the satellite dwell time is just slightly longer than the lower limit. Therefore, other data sets, like Cluster (Gustafsson et al., 1997), Magnetospheric Multiscale (Burch et al., 2016), and Arase (Miyoshi et al., 2018) satellites, are still required for more convincing statistical analysis.

Previous literature has indicated that when the solar wind ram pressure is significantly enhanced, there are two minimum-B pockets in the relatively higher latitudes, which could be another source region of chorus waves (Kim et al., 2008; Öztürk & Wolf, 2007; Shabansky, 1971; Tsurutani & Smith, 1977; Tsurutani et al., 2009). However, only the source region near the equator has been identified in our study. One of the potential reasons could be that the detection region of Van Allen Probes is in the relatively inner L-shells with $L < 6.5$, where the magnetic field lines are not significantly distorted by the solar wind pressure (Tsurutani & Smith, 1977). To investigate the more distant magnetosphere, we have also used the data from THEMIS satellites, which cover the L-shells = 5–10 (Cully et al., 2009). Nevertheless, THEMIS satellites cannot provide information of Poynting fluxes, and the waveform burst data are insufficient to provide statistically significant results (Bonnell et al., 2008; Le Contel et al., 2008). Cluster satellites are confined to the ± 30° MLAT and L-shell ≤ 7 (Cornilleau-Wehrlin et al., 2003; Gustafsson et al., 1997). They cannot provide the waveforms of electric and magnetic fields simultaneously, so we cannot analyze the wave source by calculating the Poynting fluxes. Although the Spatio-Temporal Analysis

of Field Fluctuations Spectrum Analyzer (STAFF-SA) experiment on Cluster can provide the complete spectral components data, these data are not widely available. O. Agapitov et al. (2011) used the Cluster satellites to study the chorus wave, showing no high-latitude source region of chorus waves.

Chorus has been shown to exist all the way to $L \sim 10$ by other spacecraft studies (Meredith et al., 2003; Tsurutani & Smith, 1977). For these distant regions of the outer magnetosphere, enhanced solar wind ram pressure can not only create high-latitude minimum-B pockets, but the betatron acceleration of preexisting energetic electrons in low magnetic latitudes will be considerably stronger ($\delta B/B_0$ will be large). The relative magnetic compression at the Van Allen Probes location ($L < 6$) is relatively weak because of the ambient high magnetic fields in these regions. Thus, it is possible that stronger chorus may be found during high P_d^* events if one examines larger L dayside regions that the Van Allen Probes cannot. It is also a wish that future spacecraft will be designed to go to both larger L and higher magnetic latitudes to study energetic electrons and chorus in minimum-B pockets. The wave–particle interactions in these distant regions of the magnetosphere have not been properly studied due to the lack of satellite access. Tsurutani et al. (2015) have shown that dayside plasmaspheric hiss is an order of magnitude more intense during high solar wind ram pressure intervals. If their interpretation that the hiss is chorus propagating into the plasmasphere is correct, this may indicate that chorus is most intense in the distant dayside magnetosphere during high solar wind ram pressure interval. However, without proper satellite orbits to study these occasions, we are unable to settle this issue.

Data Availability Statement

The data from Van Allen Probe A are obtained from https://spdf.gsfc.nasa.gov/pub/data/rbsp. The AE and P_d indices data are from the OMNI website (https://omniweb.gsfc.nasa.gov).

Acknowledgments
This work was supported by the Strategic Priority Research Program of the Chinese Academy of Sciences Grant XDB41000000, Key Research Program of Frontier Sciences CAS (QYZDJ-SSW-DQC010), the Fundamental Research Funds for the Central Universities (WK3420000013), and "USTC Tang Scholar" program, the China Postdoctoral Science Foundation (Grant 2021M703056). The authors acknowledge the entire Van Allen Probes team, and the data are obtained from spdf.gsfc.nasa.gov. We also acknowledge the use of NASA/GSFC's Space Physics Data Facility's OMNIWeb service and OMNI data (https://omniweb.gsfc.nasa.gov).

References

Agapitov, O., Krasnoselskikh, V., Khotyaintsev, Y. V., & Rolland, G. (2011). A statistical study of the propagation characteristics of whistler waves observed by Cluster. *Geophysical Research Letters*, *38*, L20103. https://doi.org/10.1029/2011GL049597

Agapitov, O. V., Artemyev, A. V., Mourenas, D., Mozer, F. S., & Krasnoselskikh, V. (2015). Empirical model of lower band chorus wave distribution in the outer radiation belt. *Journal of Geophysical Research: Space Physics*, *120*, 10425–10442. https://doi.org/10.1002/2015JA021829

Anderson, B. J., & Hamilton, D. C. (1993). Electromagnetic ion-cyclotron waves stimulated by modest magnetospheric compressions. *Journal of Geophysical Research*, *98*(A7), 11369–11382. https://doi.org/10.1029/93JA00605

Aryan, H., Yearby, K., Balikhin, M., Agapitov, O., Krasnoselskikh, V., & Boynton, R. (2014). Statistical study of chorus wave distributions in the inner magnetosphere using Ae and solar wind parameters. *Journal of Geophysical Research: Space Physics*, *119*, 6131–6144. https://doi.org/10.1002/2014JA019939

Bonnell, J. W., Mozer, F. S., Delory, G. T., Hull, A. J., Ergun, R. E., Cully, C. M., et al. (2008). The Electric Field Instrument (EFI) for THEMIS. *Space Science Reviews*, *141*, 303–341. https://doi.org/10.1007/s11214-008-9469-2

Burch, J. L., Moore, T. E., Torbert, R. B., & Giles, B. L. (2016). Magnetospheric multiscale overview and science objectives. *Space Science Reviews*, *199*(1–4), 5–21. https://doi.org/10.1007/s11214-015-0164-9

Burtis, W. J., & Helliwell, R. A. (1976). Magnetospheric chorus: Occurrence patterns and normalized frequency. *Planetary and Space Science*, *24*, 1007–1024. https://doi.org/10.1016/0032-0633(76)90119-7

Chen, H., Gao, X., Lu, Q., Sauer, K., Chen, R., Yao, J., & Wang, S. (2021). Gap formation around 0.5 Ωe of whistler-mode waves excited by electron temperature anisotropy. *Journal of Geophysical Research: Space Physics*, *126*, e2020JA028631. https://doi.org/10.1029/2020JA028631

Chen, H., Gao, X., Lu, Q., Tsurutani, B. T., & Wang, S. (2020). Statistical evidence for EMIC wave excitation driven by substorm injection and enhanced solar wind pressure in the Earth's magnetosphere: Two different EMIC wave sources. *Geophysical Research Letters*, *47*, e2020GL090275. https://doi.org/10.1029/2020GL090275

Chen, H. Y., Gao, X. L., Lu, Q. M., Fan, K., Ke, Y. G., Wang, X. Y., & Wang, S. (2022). Gap formation around 0.5 Omega(e) in the whistler-mode waves due to the plateau-like shape in the parallel electron distribution: 2D PIC simulations. *Journal of Geophysical Research: Space Physics*, *127*, e2021JA030119. https://doi.org/10.1029/2021JA030119

Chen, H. Y., Lu, Q. M., Wang, X. Y., Fan, K., Chen, R., & Gao, X. L. (2022). One-dimensional gcPIC-delta f simulation of hooked chorus waves in the Earth's inner magnetosphere. *Geophysical Research Letters*, *49*, e2022GL097989. https://doi.org/10.1029/2022GL097989

Chen, R., Tsurutani, B. T., Gao, X. L., Lu, Q. M., Chen, H. Y., Lakhina, G. S., & Hajra, R. (2022). The structure and microstructure of rising-tone chorus with frequencies crossing at $f \sim 0.5\, f_{ce}$. *Journal of Geophysical Research: Space Physics*, *127*, e2022JA030438. https://doi.org/10.1029/2022JA030438

Cornilleau-Wehrlin, N., Chanteur, G., Perraut, S., Rezeau, L., Robert, P., Roux, A., et al. (2003). First results obtained by the Cluster STAFF experiment. *Annales Geophysicae*, *21*(2), 437–456. https://doi.org/10.5194/angeo-21-437-2003

Cully, C. M., Ergun, R. E., Stevens, K., Nammari, A., & Westfall, J. (2009). The THEMIS digital fields board. *Space Science Reviews*, *141*(14), 343–355. https://doi.org/10.1007/s11214-008-9417-1

DeForest, S. E., & McIlwain, C. E. (1971). Plasma clouds in the magnetosphere. *Journal of Geophysical Research*, *76*(16), 3587–3611. https://doi.org/10.1029/JA076i016p03587

Fu, H., Cao, J., Mozer, F., Lu, H., & Yang, B. (2012). Chorus intensification in response to interplanetary shock. *Journal of Geophysical Research*, *117*, A01203. https://doi.org/10.1029/2011JA016913

Funsten, H. O., Skoug, R. M., Guthrie, A. A., MacDonald, E. A., Baldonado, J. R., Harper, R. W., et al. (2013). Helium, Oxygen, Proton, and Electron (HOPE) Mass Spectrometer for the radiation belt storm probes mission. *Space Science Reviews*, *179*(1–4), 423–484. https://doi.org/10.1007/s11214-013-9968-7

Gail, W., & Inan, U. (1990). Characteristics of wave–particle interactions during sudden commencements: 2. Spacecraft observations. *Journal of Geophysical Research*, *95*(A1), 139–147. https://doi.org/10.1029/JA095iA01p00139

Gail, W., Inan, U., Helliwell, R., Carpenter, D., Krishnaswamy, S., Rosenberg, T., & Lanzerotti, L. (1990). Characteristics of wave–particle interactions during sudden commencements: 1. Ground-based observations. *Journal of Geophysical Research*, *95*(A1), 119–137. https://doi.org/10.1029/JA095iA01p00119

Gao, X., Chen, L., Li, W., Lu, Q., & Wang, S. (2019). Statistical results of the power gap between lower-band and upper-band chorus waves. *Geophysical Research Letters*, *46*, 4098–4105. https://doi.org/10.1029/2019GL082140

Gao, X., Li, W., Thorne, R. M., Bortnik, J., Angelopoulos, V., Lu, Q., et al. (2014a). New evidence for generation mechanisms of discrete and hiss-like whistler mode waves. *Geophysical Research Letters*, *41*, 4805–4811. https://doi.org/10.1002/2014GL060707

Gao, X., Li, W., Thorne, R. M., Bortnik, J., Angelopoulos, V., Lu, Q., et al. (2014b). Statistical results describing the bandwidth and coherence coefficient of whistler mode waves using THEMIS waveform data. *Journal of Geophysical Research: Space Physics*, *119*, 8992–9003. https://doi.org/10.1002/2014JA020158

Gao, X., Lu, Q., & Wang, S. (2018). Statistical results of multiband chorus by using THEMIS waveform data. *Journal of Geophysical Research: Space Physics*, *123*, 5506–5515. https://doi.org/10.1029/2018JA025393

Golden, D., Spasojevic, M., Li, W., & Nishimura, Y. (2012). An empirical model of magnetospheric chorus amplitude using solar wind and geomagnetic indices. *Journal of Geophysical Research*, *117*, A12204. https://doi.org/10.1029/2012JA018210

Gustafsson, G., Boström, R., Holback, B., Holmgren, G., Lundgren, A., Stasiewicz, K., et al. (1997). The electric field and wave experiment for the Cluster mission. *Space Science Reviews*, *79*(1–2), 137–156. https://doi.org/10.1023/A:1004975108657

Hajra, R. B., Tsurutani, T., Echer, E., Gonzalez, W. D., & Santolik, O. (2015). Relativistic ($E > 0.6$, >2.0, and >4.0 MeV) electron acceleration at geosynchronous orbit during high-intensity long-duration, continuous AE activity (HILDCAA) events. *The Astrophysical Journal*, *799*, 39. https://doi.org/10.1088/0004-637X/799/1/39

Helliwell, R. A. (1965). *Whistlers and related ionospheric phenomena.* Stanford University Press.

Keika, K., Spasojevic, M., Li, W., Bortnik, J., Miyoshi, Y., & Angelopoulos, V. (2012). PENGUIn/AGO and THEMIS conjugate observations of whistler mode chorus waves in the dayside uniform zone under steady solar wind and quiet geomagnetic conditions. *Journal of Geophysical Research*, *117*, A07212. https://doi.org/10.1029/2012JA017708

Kennel, C. F., & Petschek, H. E. (1966). Limit on stably trapped particle fluxes. *Journal of Geophysical Research*, *71*(1), 1–28. https://doi.org/10.1029/JZ071i001p00001

Kessel, R., Fox, N., & Weiss, M. (2013). The Radiation Belt Storm Probes (RBSP) and space weather. *Space Science Reviews*, *179*(1–4), 531–543. https://doi.org/10.1007/s11214-012-9953-6

Kim, K. C., Lee, D. Y., Kim, H. J., Lyons, L. R., Lee, E., Öztürk, M. K., & Choi, C. (2008). Numerical calculations of relativistic electron drift loss effect. *Journal of Geophysical Research*, *113*, A09212. https://doi.org/10.1029/2007JA013011

Kim, K. C., Shprits, Y., Lee, J., & Hwang, J. (2013). Empirically modeled global distribution of magnetospheric chorus amplitude using an artificial neural network. *Journal of Geophysical Research: Space Physics*, *118*, 6243–6253. https://doi.org/10.1002/jgra.50595

Kletzing, C. A., Kurth, W. S., Acuna, M., MacDowall, R. J., Torbert, R. B., Averkamp, T., et al. (2013). The Electric and Magnetic Field Instrument Suite and Integrated Science (EMFISIS) on RBSP. *Space Science Reviews*, *179*, 127–181. https://doi.org/10.1007/s11214-013-9993-6

Koons, H. C., & Roeder, J. L. (1990). A survey of equatorial magnetospheric wave activity between 5 and 8 RE. *Planetary and Space Science*, *38*(10), 1335–1341. https://doi.org/10.1016/0032-0633(90)90136-E

Kubota, Y., Omura, Y., Kletzing, C., & Reeves, G. (2018). Generation process of large-amplitude upper-band chorus emissions observed by Van Allen Probes. *Journal of Geophysical Research: Space Physics*, *123*, 3704–3713. https://doi.org/10.1029/2017JA024782

Kurth, W. S., De Pascuale, S., Faden, J. B., Kletzing, C. A., Hospodarsky, G. B., Thaller, S., & Wygant, J. R. (2015). Electron densities inferred from plasma wave spectra obtained by the Waves instrument on Van Allen Probes. *Journal of Geophysical Research: Space Physics*, *120*, 904–914. https://doi.org/10.1002/2014JA020857

Lauben, D. S., Inan, U. S., Bell, T. F., & Gurnett, D. A. (2002). Source characteristics of ELF/VLF chorus. *Journal of Geophysical Research*, *107*(A12), 1429. https://doi.org/10.1029/2000JA003019

Le Contel, O., Roux, A., Robert, P., Coillot, C., Bouabdellah, A., de la Porte, B., et al. (2008). First results of the THEMIS Search Coil Magnetometers. *Space Science Reviews*, *141*, 509–534. https://doi.org/10.1007/s11214-008-9371-y

LeDocq, M. J., Gurnett, D. A., & Hospodarsky, G. B. (1998). Chorus source locations from VLF Poynting flux measurements with the Polar spacecraft. *Geophysical Research Letters*, *25*(21), 4063–4066. https://doi.org/10.1029/1998GL900071

Li, W., Santolik, O., Bortnik, J., Thorne, R. M., Kletzing, C. A., Kurth, W. S., & Hospodarsky, G. B. (2016). New chorus wave properties near the equator from Van Allen Probes wave observations. *Geophysical Research Letters*, *43*, 4725–4735. https://doi.org/10.1002/2016GL068780

Li, W., Thorne, R. M., Angelopoulos, V., Bonnell, J. W., McFadden, J. P., Carlson, C. W., et al. (2009). Evaluation of whistler-mode chorus intensification on the nightside during an injection event observed on the THEMIS spacecraft. *Journal of Geophysical Research*, *114*, A00C14. https://doi.org/10.1029/2008JA013554

Li, W., Thorne, R. M., Angelopoulos, V., Bortnik, J., Cully, C. M., Ni, B., et al. (2009). Global distribution of whistler-mode chorus waves observed on the THEMIS spacecraft. *Geophysical Research Letters*, *36*, L09104. https://doi.org/10.1029/2009GL037595

Li, W., Thorne, R. M., Bortnik, J., Tao, X., & Angelopoulos, V. (2012). Characteristics of hiss-like and discrete whistler-mode emissions. *Geophysical Research Letters*, *39*, L18106. https://doi.org/10.1029/2012GL053206

Li, W., Thorne, R. M., Nishimura, Y., Bortnik, J., Angelopoulos, V., McFadden, J. P., et al. (2010). THEMIS analysis of observed equatorial electron distributions responsible for the chorus excitation. *Journal of Geophysical Research*, *115*, A00F11. https://doi.org/10.1029/2009JA014845

Liu, S., Xia, Z., Chen, L., Liu, Y., Liao, Z., & Zhu, H. (2019). Magnetospheric multiscale observation of quasiperiodic EMIC waves associated with enhanced solar wind pressure. *Geophysical Research Letters*, *46*, 7096–7104. https://doi.org/10.1029/2019GL083421

Lopez, R. E., Sibeck, D. G., McEntire, R. W., & Krimigis, S. M. (1990). The energetic ion substorm injection boundary. *Journal of Geophysical Research*, *95*(A1), 109–117. https://doi.org/10.1029/JA095iA01p00109

Lu, Q., Chen, L., Wang, X., Gao, X., Lin, Y., & Wang, S. (2021). Repetitive emissions of rising-tone chorus waves in the inner magnetosphere. *Geophysical Research Letters*, *48*, e2021GL094979. https://doi.org/10.1029/2021GL094979

Lu, Q., Ke, Y., Wang, X., Liu, K., Gao, X., Chen, L., & Wang, S. (2019). Two-dimensional general curvilinear particle-in-cell (gcPIC) simulation of rising-tone chorus waves in a dipole magnetic field. *Journal of Geophysical Research: Space Physics*, *124*, 4157–4167. https://doi.org/10.1029/2019JA026586

Mauk, B. H., Fox, N. J., Kanekal, S. G., Kessel, R. L., Sibeck, D. G., & Ukhorskiy, A. (2013). Science objectives and rationale for the radiation belt storm probes mission. *Space Science Reviews*, *179*(1), 3–27. https://doi.org/10.1007/s11214-012-9908-y

Meredith, N. P., Horne, R. B., Sicard-Piet, A., Boscher, D., Yearby, K. H., Li, W., & Thorne, R. M. (2012). Global model of lower band and upper band chorus from multiple satellite observations. *Journal of Geophysical Research*, *117*, A10225. https://doi.org/10.1029/2012JA017978

Meredith, N. P., Horne, R. B., Thorne, R. M., & Anderson, R. R. (2003). Favored regions for chorus-driven electron acceleration to relativistic energies in the Earth's outer radiation belt. *Geophysical Research Letters*, *30*(16), 1871. https://doi.org/10.1029/2003GL017698

Min, K., Lee, J., & Keika, K. (2010). Chorus wave generation near the dawnside magnetopause due to drift shell splitting of substorm-injected electrons. *Journal of Geophysical Research*, *115*, A00I02. https://doi.org/10.1029/2010JA015474

Miyoshi, Y., Morioka, A., Kataoka, R., Kasahara, Y., & Mukai, T. (2007). Evolution of the outer radiation belt during the November 1993 storms driven by corotating interaction regions. *Journal of Geophysical Research*, *112*, A05210. https://doi.org/10.1029/2006JA012148

Miyoshi, Y., Shinohara, I., Takashima, T., Asamura, K., Higashio, N., Mitani, T., et al. (2018). Geospace exploration project ERG. *Earth Planets and Space*, *70*, 101. https://doi.org/10.1186/s40623-018-0862-0

Nishimura, Y., Bortnik, J., Li, W., Thorne, R. M., Lyons, L. R., Angelopoulos, V., et al. (2010). Identifying the driver of pulsating aurora. *Science*, *330*, 81–84. https://doi.org/10.1126/science.1193186

Omura, Y. (2021). Nonlinear wave growth theory of whistler-mode chorus and hiss emissions in the magnetosphere. *Earth Planets and Space*, *73*(1), 95. https://doi.org/10.1186/s40623-021-01380-w

Omura, Y., Katoh, Y., & Summers, D. (2008). Theory and simulation of the generation of whistler-mode chorus. *Journal of Geophysical Research*, *113*, A04223. https://doi.org/10.1029/2007JA012622

Öztürk, M. K., & Wolf, R. A. (2007). Bifurcation of drift shells near the dayside magnetopause. *Journal of Geophysical Research*, *112*, A07207. https://doi.org/10.1029/2006JA012102

Roederer, J. G. (1967). On the adiabatic motion of energetic particles in a model magnetosphere. *Journal of Geophysical Research*, *72*(3), 981–992. https://doi.org/10.1029/JZ072i003p00981

Salvati, M., Inan, U., Rosenberg, T., & Weatherwax, A. (2000). Solar wind control of polar chorus. *Geophysical Research Letters*, *27*(5), 649–656. https://doi.org/10.1029/1999GL010702

Shabansky, V. (1971). Some processes in the magnetosphere. *Space Science Reviews*, *12*(3), 299–418. https://doi.org/10.1007/BF00165511

Sheeley, B. W., Moldwin, M. B., Rassoul, H. K., & Anderson, R. R. (2001). An empirical plasmasphere and trough density model: CRRES observations. *Journal of Geophysical Research*, *106*(A11), 25631–25641. https://doi.org/10.1029/2000JA000286

Southwood, D. J., & Kivelson, M. G. (1975). Approximate analytic description of plasma bulk parameters and pitch angle anisotropy under adiabatic flow in a dipolar magnetospheric field. *Journal of Geophysical Research*, *80*(16), 2069–2073. https://doi.org/10.1029/JA080i016p02069

Spasojevic, M., & Inan, U. S. (2010). Drivers of chorus in the outer dayside magnetosphere. *Journal of Geophysical Research*, *115*, A00F09. https://doi.org/10.1029/2009JA014452

Taubenschuss, U., Santolik, O., Breuillard, H., Li, W., & Le Contel, O. (2016). Poynting vector and wave vector directions of equatorial chorus. *Journal of Geophysical Research: Space Physics*, *121*, 11912–11928. https://doi.org/10.1002/2016JA023389

Teng, S., Tao, X., Li, W., Qi, Y., Gao, X., Dai, L., et al. (2018). A statistical study of the spatial distribution and source-region size of chorus waves using Van Allen Probes data. Paper presented at Annales Geophysicae. Copernicus GmbH. https://doi.org/10.5194/angeo-36-867-2018

Thorne, R. M. (2010). Radiation belt dynamics: The importance of wave-particle interactions. *Geophysical Research Letters*, *37*, L22107. https://doi.org/10.1029/2010GL044990

Thorne, R. M., & Kennel, C. F. (1967). Quasi-trapped VLF propagation in the outer magnetosphere. *Journal of Geophysical Research*, *72*(3), 857–870. https://doi.org/10.1029/JZ072i003p00857

Thorne, R. M., Li, W., Ni, B., Ma, Q., Bortnik, J., Chen, L., et al. (2013). Rapid local acceleration of relativistic radiation-belt electrons by magnetospheric chorus. *Nature*, *504*, 411–414. https://doi.org/10.1038/nature12889

Thorne, R. M., Ni, B., Tao, X., Horne, R. B., & Meredith, N. P. (2010). Scattering by chorus waves as the dominant cause of diffuse auroral precipitation. *Nature*, *467*, 943–946. https://doi.org/10.1038/nature09467

Tsurutani, B. T., Chen, R., Gao, X. L., Lu, Q. M., Pickett, J. S., Lakhina, G. S., et al. (2020). Lower-band "monochromatic" chorus riser subelement/wave packet observations. *Journal of Geophysical Research: Space Physics*, *125*, e2020JA028090. https://doi.org/10.1029/2020JA028090

Tsurutani, B. T., Church, S. R., & Thorne, R. M. (1979). Search for geographic control on the occurrence of magnetospheric ELF emissions. *Journal of Geophysical Research*, *84*(A8), 4116–4124. https://doi.org/10.1029/JA084iA08p04116

Tsurutani, B. T., Falkowski, B. J., Pickett, J. S., Santolik, O., & Lakhina, G. S. (2015). Plasmaspheric hiss properties: Observations from polar. *Journal of Geophysical Research: Space Physics*, *120*, 414–431. https://doi.org/10.1002/2014JA020518

Tsurutani, B. T., & Lakhina, G. S. (1997). Some basic concepts of wave–particle interactions in collisionless plasmas. *Reviews of Geophysics*, *35*(4), 491–502. https://doi.org/10.1029/97RG02200

Tsurutani, B. T., Lakhina, G. S., & Verkhoglyadova, O. P. (2013). Energetic electron (>10 keV) microburst precipitation, similar to 5–15 s X-ray pulsations, chorus, and wave–particle interactions: A review. *Journal of Geophysical Research: Space Physics*, *118*, 2296–2312. https://doi.org/10.1002/jgra.50264

Tsurutani, B. T., & Smith, E. J. (1974). Postmidnight chorus: A substorm phenomenon. *Journal of Geophysical Research*, *79*(1), 118–127. https://doi.org/10.1029/JA079i001p00118

Tsurutani, B. T., & Smith, E. J. (1977). Two types of magnetospheric ELF chorus and their substorm dependences. *Journal of Geophysical Research*, *82*(32), 5112–5128. https://doi.org/10.1029/JA082i032p05112

Tsurutani, B. T., Smith, E. J., West, H. I., Jr., & Buck, R. M. (1979). Chorus, energetic electrons and magnetospheric substorms. In P. J. Palmadesso & K. Papadopoulos (Eds.), *Wave instabilities in space plasmas* (Vol. 55–71, pp. 55–62). Amsterdam: D. Reidel. https://doi.org/10.1007/978-94-009-9500-0_6

Tsurutani, B. T., Verkhoglyadova, O. P., Lakhina, G. S., & Yagitani, S. (2009). Properties of dayside outer zone chorus during HILDCAA events: Loss of energetic electrons. *Journal of Geophysical Research*, *114*, A03207. https://doi.org/10.1029/2008JA013353

Tsyganenko, N., & Sitnov, M. (2005). Modeling the dynamics of the inner magnetosphere during strong geomagnetic storms. *Journal of Geophysical Research*, *110*, A03208. https://doi.org/10.1029/2004JA010798

Tu, W., Cunningham, G. S., Chen, Y., Morley, S. K., Reeves, G. D., Blake, J. B., et al. (2014). Event-specific chorus wave and electron seed population models in DREAM3D using the Van Allen Probes. *Geophysical Research Letters*, *41*, 1359–1366. https://doi.org/10.1002/2013GL058819

Vaivads, A., Santolík, O., Stenberg, G., André, M., Owen, C., Canu, P., & Dunlop, M. (2007). Source of whistler emissions at the dayside magnetopause. *Geophysical Research Letters*, *34*, L09106. https://doi.org/10.1029/2006GL029195

Verkhoglyadova, O. P., Tsurutani, B. T., & Lakhina, G. S. (2010). Properties of obliquely propagating chorus. *Journal of Geophysical Research*, *115*, A00F19. https://doi.org/10.1029/2009JA014809

Wang, D., Shprits, Y. Y., Zhelavskaya, I. S., Agapitov, O. V., Drozdov, A. Y., & Aseev, N. A. (2019). Analytical chorus wave model derived from Van Allen Probe observations. *Journal of Geophysical Research: Space Physics*, *124*, 1063–1084. https://doi.org/10.1029/2018JA026183

West, H., Jr., Buck, R., & Walton, J. (1973). Electron pitch angle distributions throughout the magnetosphere as observed on Ogo 5. *Journal of Geophysical Research*, *78*(7), 1064–1081. https://doi.org/10.1029/JA078i007p01064